Structural Influence of the Cabin Floor on Sound Transmission into Aircraft—Analytical Investigations

C. R. Fuller*
Virginia Polytechnic Institute and State University, Blacksburg, Virginia

The structural influence of the cabin floor on the transmission of low-frequency propeller noise into aircraft interiors has been examined using a simplified analytical model. The response amplitudes and distributions of shell displacement and internal acoustic pressure are examined for various frequencies and floor configurations. In general, at lower frequencies, the floor exerts little structural influence on the transmission of acoustic energy to the interior. However, as the frequency nears half the cylinder ring frequency, the floor can be seen to alter significantly the internal pressure distributions and response.

Nomenclature

a = shell mean radius
A_n,B_n = shell displacement modal amplitudes
c_L = shell extensional phase speed
F = half-number of floor attachment points
$F_{\ell f}$ = point force amplitudes
h = shell wall thickness
I = intensity
I_{33} = (3,3) element of inverse matrix (from Ref. 1)
J_n,H_n = Bessel and Hankel functions
k_n,k_r = axial and radial wavenumbers (from Ref. 1)
M = total number of angles in modal decomposition
n = circumferential mode number
p = acoustic pressure
p_0 = source pressure amplitude
r,θ,x = cylindrical coordinates
R_s = source position (component)
w = shell displacement
x_f = axial coordinate of attachment point
x_p = floor attachment spacing
$\Delta\theta$ = angle increment of modal decomposition
ε = 2 if $n=0$, = 1 if $n>0$
ε_n = 1 if $n=0$, = 2 if $n>0$
ρ_f = density of fluid medium
ρ_s = density of shell medium
ϕ_s = phase lead of source component
Ω = nondimensional source frequency, $=\omega a/c_L$
ω = source frequency

Subscripts

d = dipole
f = attachment point index (axial)
fo = force
j,z = equation indices
ℓ = attachment point index (angle)
m = decomposition point index
s = source component

Presented as Paper 86-1940 at the AIAA 10th Aeroacoustics Conference, Seattle, WA, July 9–11, 1986; received Oct. 22, 1986; revision received March 16, 1987. Copyright © American Institute of Aeronautics and Astronautics, Inc., 1987. All rights reserved.

*Associate Professor of Mechanical Engineering. Member AIAA.

Introduction

PREVIOUS work[1] has been concerned with developing an analytical model for investigating sound transmission into the cabins of propeller aircraft. The analytical model has proved successful in uncovering various mechanisms inherent in the transmission phenomena.[2,3] However, the analytical model for these investigations consisted of a homogenous cylindrical shell, and experimental work[4] in which an aircraft fuselage was modeled by a finite, closed cylindrical shell has indicated that discontinuities in the shell structure lead to a marked change in the shell response.

Because the cabin floor represents a most definite departure from homogeneity, it was felt necessary to introduce the dynamics of the cabin floor into the analytical model. An outcome of this development of the model is the ability to study the effect of the floor on the sound transmission into aircraft interiors. The main influences of the floor are due to a structural modification of the fuselage response and a modification of the interior acoustic space due to an extra radiating surface. For this investigation, one mechanism is isolated; since the influence of the floor is limited to a structural case, the floor is considered acoustically transparent.

Hence, the aim of this paper is to study analytically the structural influence of the cabin floor on aircraft interior noise, using a simplified mathematical representation of the aircraft. For the analysis presented here, the fuselage is represented as an infinite thin-walled cylindrical shell with a coupled interior acoustic field. This model is appropriate in light of measurements showing that vibration levels on a typical aircraft fuselage decrease with the distance away from the propeller plane.[5] As previously used,[1] the acoustic excitation due to the exterior propellers is represented by a dipole placed at the correct location to give a representative pressure distribution on the cylinder exterior. In this paper, only one propeller is modeled in order to eliminate any additional effects due to synchrophasing.

In typical aircraft configurations, the cabin floor is attached to fuselage ribs. Thus, for this analysis, the floor is considered as a series of periodic point attachments to the shell wall. This arrangement considers only the structural influence of the floor; any scattering from the floor surface itself is not included. Likewise, the floor exerts an influence only on the radial motion of the cylinder; the effects of altering bending moment and in-plane shell motion are not considered. The location of the attachment points is determined by the floor width and rib spacing. Previous work[6] has demonstrated that the floor effectively forces a node in the distribution of radial shell vibration at each attachment location. Thus, the

boundary condition used in the analysis is that the shell radial displacement is zero at each attachment point.

To find an analytical solution to the situation, the problem is split into two parts. First, the response of the homogeneous shell to the exterior dipole is derived.[1] Next, the response of the shell to the series of point forces is obtained using equations similar to those employed by James.[7] The response to the complete system is then obtained, on the basis of linear superposition, by adding the two separate solutions. Implementation of the boundary condition of zero radial displacement at each attachment point enables the complex amplitude of each force to be obtained (there necessarily must be a finite number of forces). On resubstitution of the forces back into the complete equations of motion, the shell displacement, interior pressure field, acoustic intensity vectors at the shell wall interior, and power flow into the interior cavity can be evaluated. Setting the forces to zero enables the structural effect of the floor to be removed and, thus, its influence on the major transmission phenomena can be readily studied. The work is being carried out in conjunction with an experimental investigation.[8]

Analysis

The cylindrical coordinate system and the geometry employed in the analysis are shown in Fig. 1. The response of the system to each component will first be derived. Then the coupled solution is obtained.

Dipole Source

As derived in Ref. 1, the radial displacement response of the cylindrical shell to the external dipole, located at $\theta = 0$, $r = R_s$ can be written as

$$\omega_d = \frac{\Omega^2}{\pi\rho_s h a\omega^2} p_0 \sum_{s=1}^{2} \exp[i\phi_s] \sum_{n=0}^{\infty} \varepsilon_n \cos(n\theta) \times \int_{-\infty}^{\infty} \frac{H_n(k_r R_s)}{H_n'(k_r a) k_r a} I_{33} \exp\left[i(k_n a)\left(\frac{x}{a}\right)\right] \mathrm{d}(k_n a) \tag{1}$$

where the expansion of I_{33} is given in Ref. 1.

Point Force

The response of the system to a radial point force located at θ_ℓ, x_f is[7]

$$\omega_{fo} = -\frac{\Omega^2}{2\pi\rho_s h a\omega^2} F_{\ell f} \sum_{n=0}^{\infty} \varepsilon_n \cos(n\theta - n\theta_\ell) \times \int_{-\infty}^{\infty} I_{33} \exp\left\{ i\left[k_n a\left(\frac{x}{a} - \frac{x_f}{a}\right)\right]\right\} \mathrm{d}(k_n a) \tag{2}$$

Floor Model

As shown in Fig. 1, the structural effect of the floor is modeled as two lines of periodic forces on each side of the shell at angles of $-\theta_f$ and $\pi + \theta_f$.

Let the number of forces along one line be an odd number denoted F. If the middle force is assumed positioned at the system centerline, $x/a = 0$, then the axial location of each force, $f = 1$ to F, can be calculated from

$$x_f = (x_p/a)(F/2 - f + 0.5) \tag{3}$$

where x_p/a is the nondimensional axial spacing of each attachment point.

Thus, the shell radial response to a set of $2F$ forces as shown in Fig. 1 can be written as

$$\omega_{fo}^{\text{total}} = \frac{\Omega^2}{2\pi\rho_s h a w^2} \sum_{\ell=1}^{2} \sum_{f=1}^{F} F_{\ell f} \sum_{n=0}^{\infty} \varepsilon_n \cos(n\theta - n\theta_\ell) \times \int_{-\infty}^{\infty} I_{33} \exp\left\{ i\left[k_n a\left(\frac{x}{a} - \frac{x_f}{a}\right)\right]\right\} \mathrm{d}(k_n a) \tag{4}$$

Hence, the total radial vibration of the system to the point forces and the dipoles can be written as

$$\omega_{\text{total}}\left(\theta, \frac{x}{a}\right) = \frac{\Omega^2}{\pi\rho_s h a\omega^2}\left[p_0 \sum_{s=1}^{2} \exp[i\phi_s] \sum_{n=0}^{\infty} \varepsilon_n \cos(n\theta) \times \int_{-\infty}^{\infty} \frac{H_n(k_r R_s)}{H_n'(k_r a) k_r a} I_{33} \exp\left[i(k_n a)\left(\frac{x}{a}\right)\right] \mathrm{d}(k_n a) - \frac{1}{2} \sum_{\ell=1}^{2} \sum_{f=1}^{F} F_{\ell f} \sum_{n=0}^{\infty} \varepsilon_n \cos(n\theta - n\theta_\ell) \times \int_{-\infty}^{\infty} I_{33} \exp\left\{ i\left[k_n a\left(\frac{x}{a} - \frac{x_f}{a}\right)\right]\right\} \mathrm{d}(k_n a)\right] \tag{5}$$

The next step in the analysis is to obtain the unknown complex force amplitudes $F_{\ell f}$. If we assume that we have $2F$ unknown force amplitudes, then application of the boundary condition of zero radial shell displacement at each force location results in $2F$ equations and the problem can be solved using simultaneous equations.

Hence, applying the boundary condition that

$$\omega_{\text{total}}\Big|_{\substack{x = x_j \\ \theta = \theta_z}} = 0 \tag{6}$$

gives $2F$ equations at each force location such that

$$\sum_{\ell=1}^{2} \sum_{f=1}^{F} F_{\ell f} \sum_{n=0}^{\infty} \varepsilon_n \cos(n\theta_z - n\theta_\ell) \times \int_{-\infty}^{\infty} I_{33} \exp\left\{ i\left[k_n a\left(\frac{x_j}{a} - \frac{x_f}{a}\right)\right]\right\} \mathrm{d}(k_n a) = -2 \sum_{s=1}^{2} p_0 \exp[i\phi_s] \sum_{n=0}^{\infty} \varepsilon_n \cos(n\theta_z) \times \int_{-\infty}^{\infty} I_{33} \exp\left\{ i\left[k_n a\left(\frac{x_j}{a} - \frac{x_f}{a}\right)\right]\right\} \mathrm{d}(k_n a) \tag{7}$$

for $j = 1$ to F and $z = 1$ to 2.

Application of the boundary condition as outlined above can be seen to result in $2F$ simultaneous equations with $2F$ unknown force amplitudes. By assuming a value for the source amplitude p_0, the complex force amplitudes can be solved using standard matrix theory. The total radial vibrational displacement of the system at (x,θ) can then be obtained by resubstituting the force amplitudes back into Eq. (5).

The total interior acoustic pressure of the shell can also be similarly obtained from[1,7]

$$p_{\text{total}}\left(r, \theta, \frac{x}{a}\right) = \frac{1}{\pi a} \Omega^2 \left(\frac{\rho_f}{\rho_s}\right)\left(\frac{h}{a}\right)^{-1} \times \left[p_0 \sum_{s=1}^{2} \exp[i\phi_s] \sum_{n=0}^{\infty} \varepsilon_n \cos(n\theta) \times \int_{-\infty}^{\infty} \left[\frac{H_n(k_r R_s)}{H_n'(k_r a) k_r a}\right]\left[\frac{J_n(k_r r)}{J_n'(k_r a) k_r a}\right] \times I_{33} \exp\left[i(k_n a)\left(\frac{x}{a}\right)\right] \mathrm{d}(k_n a) - \frac{1}{2} \sum_{\ell=1}^{2} \sum_{f=1}^{F} F_{\ell f} \sum_{n=0}^{\infty} \varepsilon_n \cos(n\theta - n\theta_\ell) \times \int_{-\infty}^{\infty} \left[\frac{J_n(k_r r)}{J_n'(k_r a) k_r a}\right] I_{33} \times \exp\left\{ i\left[k_n a\left(\frac{x}{a} - \frac{x_f}{a}\right)\right]\right\} \mathrm{d}(k_n a)\right] \tag{8}$$

Evaluating both the shell radial response and the interior acoustic pressure at $r = a$ from Eqs. (5) and (8), respectively, allows the calculation of the time-averaged radial intensity vec-

tors at the interior of the shell wall as

$$I(\theta,x/a) = \tfrac{1}{2}\,\mathrm{Re}[p \times (\overline{-i\omega w})] \tag{9}$$

It is also of use to decompose the total shell response and total pressures obtained from Eqs. (5) and (8) into individual circumferential modes of vibrations, $A_n \cos(n\theta)$ and $B_n \sin(n\theta)$.

For example, if the total shell response is given by Eq. (5), it can also be written as

$$w = \sum_{n=0}^{\infty} A_n \cos(n\theta) + \sum_{n=0}^{\infty} B_n \sin(n\theta) \tag{10}$$

Utilizing the orthogonality of the cosine and sine functions allows the modal amplitudes to be determined as[4]

$$A_n = \frac{1}{\varepsilon\pi} \sum_{m=1}^{M} w(\theta_m) \cos(n\theta_m)\,\Delta\theta \tag{11}$$

$$B_n = \frac{1}{\varepsilon\pi} \sum_{m=1}^{M} w(\theta_m) \sin(n\theta_m)\Delta\theta \tag{12}$$

where $w(\theta_m)$ is the total shell response at angle θ_m calculated from Eq. (5), M the total number of angles considered, and $\Delta\theta$ the angle increment (or width of sampling angle). As Eqs. (11) and (12) are discrete modal decompositions, the usual aliasing conditions apply, i.e., if there are M sampled points, then the highest circumferential mode amplitude that can be decomposed is $n = M/2 - 1$.

Results and Discussions

The following results were calculated for a representative aircraft situation similar to those for proposed advanced turbopropeller (ATP) aircraft. The shell material was taken to be aluminum with a nondimensional wall thickness of $h/a = 0.002$. The shell was also assumed to be homogeneous, the stringers and ribs being "smeared" as described by Pope.[9] The propagating medium was assumed to be air at rest. Material properties are provided in Table 1.

The equivalent source locations were derived as described in Ref. 1 and were chosen such that $R_1/a = 1.8$ and $R_2/a = 1.9$. This might correspond to, for example, a 9 ft diameter propeller with a 1 ft tip clearance mounted on a 10 ft diameter fuselage, a situation representative of a medium-sized ATP aircraft. The nondimensional frequency range chosen for the investigation was $\Omega = 0.2$ to 0.5 [$\Omega = \omega a/c_L$ (see Ref. 1)] which in the 10 ft diameter fuselage represents a fundamental frequency range of 108–270 Hz, which again is the frequency range expected for the fundamental of advanced turbopropellers. The source amplitude p_0 was set to unity, as the main purpose of the work was a comparison of results rather than absolute levels.

The floor spacing was standardized at $x_p/a = 0.5$, which in the 10 ft diameter fuselage gave a rib spacing of 2.5 ft. Three different floor angles were investigated, $\theta_f = 0$, -30, and -60 deg. However, only the results for the first two angles are presented. The computational time was found to be strongly dependent upon the number of floor mount positions F. Thus, it was decided to use a finite number of forces so as to extend over the axial region of the shell where the external pressure forcing function was high. This region was found to extend approximately 2 radii on each side of the source plane and, thus, F was chosen to be 9, giving 18 attachment points. This "truncation" of the length of the floor necessitated calculation of the system response at $x/a = 0$ where the floor end effects are negligible.

It was also necessary to truncate the modal sums of Eqs. (5) and (8) and these relationships were found to converge sufficiently if 10 circumferential modes were included for the dipole part of the equations, while 15 modes were needed for the force part of the equations. The integrands were evaluated as outlined in Ref. 1 using a Gaussian quadrature integration scheme.

Table 1 Material properties

Material	Poisson's ratio	Density, kg/m^3	Free wave speed, m/s
Aluminum	0.33	2700	5150
Air	—	1.2	343

Table 2 Displacement modal decompositions ($\Omega = 0.2$, $\theta_f = -30$ deg)

	A_n		B_n	
n	No floor	Floor	No floor	floor
0	0.405×10^0	0.398×10^0	0	0
1	0.179×10^1	0.165×10^1	0	0.646×10^{-1}
2	0.324×10^1	0.321×10^1	0	0.345×10^0
3	0.749×10^1	0.749×10^1	0	0.349×10^0
4	0.533×10^1	0.530×10^1	0	0.214×10^0
5	0.209×10^1	0.184×10^1	0	0.336×10^0
6	0.842×10^0	0.423×10^0	0	0
7	0.455×10^0	0.418×10^0	0	0.563×10^0
8	0.247×10^0	0.159×10^0	0	0.394×10^0
9	0.140×10^0	0.140×10^0	0	0.383×10^0

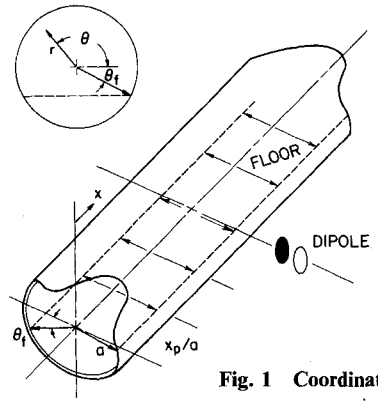

Fig. 1 Coordinate system and floor geometry.

Figure 2 shows shell relative radial displacement amplitude $w^{\mathrm{rel}} = |w_{\mathrm{total}}/[\Omega^2/\pi\rho_s h a\omega^2]|$ plotted at $x/a = 0$ for various circumferential angles. The driving frequency is $\Omega = 0.2$ and the cases of no floor and a floor angle of $\theta_f = -30$ deg are given. It is apparent that the effect of the floor is to force a node in the shell response at the attachment points, as required by the boundary condition. At other angles, the floor has only a small effect on the structural motion.

Figure 3 presents the corresponding relative interior acoustic pressure amplitude $p^{\mathrm{rel}} = |p_{\mathrm{total}}/[\Omega^2\rho_f/\pi\rho_s h a]|$ evaluated at $r/a = 0.75$ for the same conditions as Fig. 2. Surprisingly, the interior pressure distribution is little affected by the presence of the floor at all angles and appears to be dominated by the $n = 2$ circumferential mode.

In order to understand the behavior inherent in the results of Figs. 2 and 3, it is useful to perform a modal decomposition of the circumferential response in each case, using the relations of Eqs. (11) and (12). Table 2 presents relative shell radial displacement amplitude for each circumferential mode n with and without the floor present. Without the floor present, the shell responds in approximately five lower-order circumferential modes. Introducing the floor into the model leads to a generation of antisymmetric modes as well as higher-order modes ($n > 9$), with only a slight modification of the amplitude of the lower-order symmetric modes. Thus, the boundary condition of zero displacement of the attachment point is achieved by the generation of other modes without suppressing modes of vibration that already exist when the floor is present. This behavior

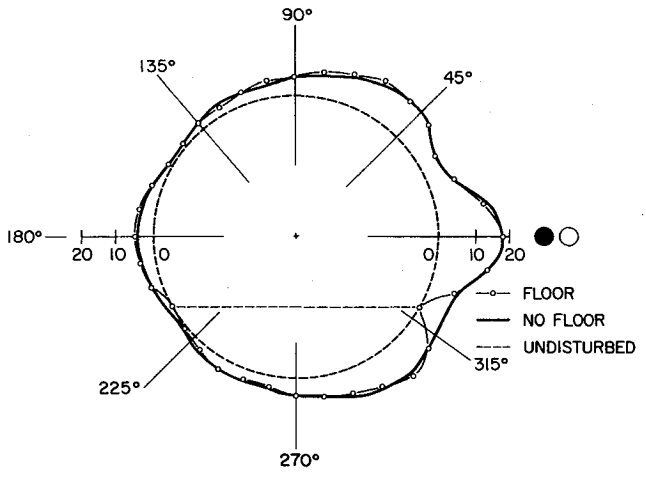

Fig. 2 Shell radial displacement amplitude ($\Omega = 0.2$, $\theta_f = -30$ deg).

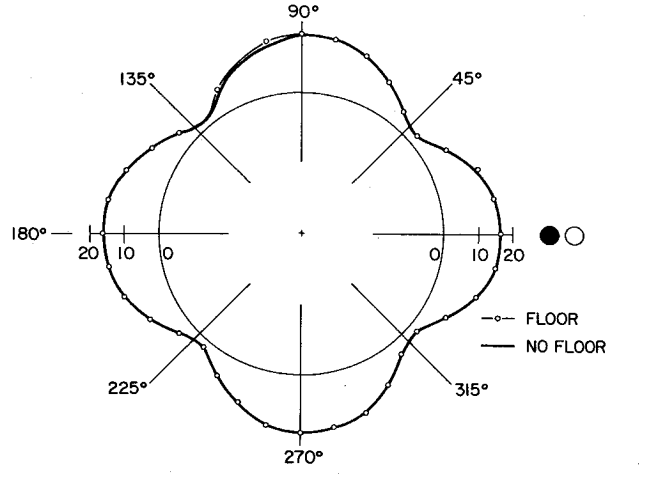

Fig. 3 Shell interior pressure amplitude ($\Omega = 0.2$, $\theta_f = -30$ deg, $r/a = 0.75$).

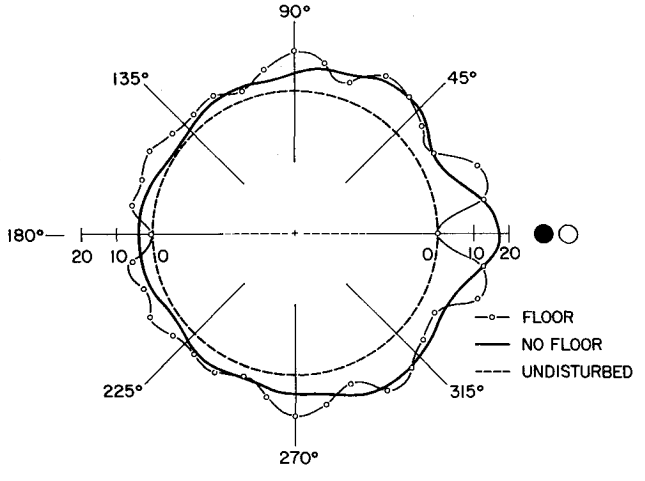

Fig. 4 Shell radial displacement amplitude ($\Omega = 0.2$, $\theta_f = 0$ deg).

is due to the infinite spectral (wavenumber domain) bandwith of the point force, as opposed to the limited bandwidth of the distributed acoustic excitation.

Table 3 gives the modal decomposition of the corresponding internal pressure field with and without the floor in place. Without the floor in place, the interior field is dominated by only *one* circumferential mode. Thus, out of the five shell

Table 3 Pressure modal decompositions ($\Omega = 0.2$, $\theta_f = -30$ deg, $r/a = 0.75$)

	A_n		B_n	
n	No floor	Floor	No floor	Floor
0	0.556×10^{-1}	0.530×10^{-1}	0	0
1	0.820×10^{0}	0.795×10^{0}	0	0.132×10^{1}
2	0.160×10^{2}	0.157×10^{2}	0	0.967×10^{0}
3	0.237×10^{1}	0.237×10^{1}	0	0.535×10^{-1}
4	0.658×10^{0}	0.654×10^{0}	0	0.111×10^{-1}
5	0.130×10^{0}	0.121×10^{0}	0	0.807×10^{-2}
6	0.298×10^{-1}	0.157×10^{-1}	0	0
7	0.953×10^{-2}	0.171×10^{-1}	0	0.197×10^{-1}
8	0.356×10^{-2}	0.136×10^{-1}	0	0.910×10^{-2}
9	0.153×10^{-2}	0.115×10^{-2}	0	0.678×10^{-2}

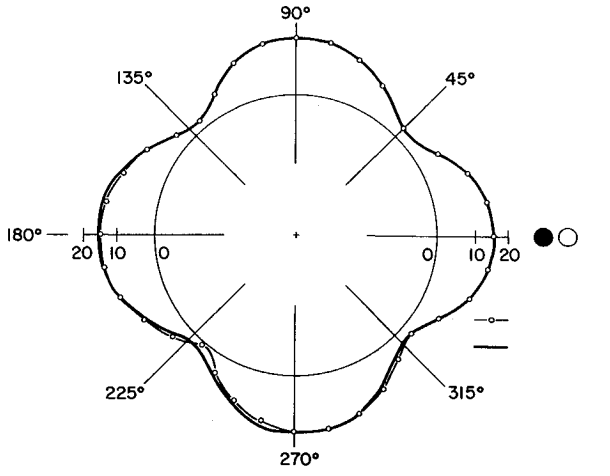

Fig. 5 Shell interior pressure amplitude ($\Omega = 0.2$, $\theta_f = 0$ deg, $r/a = 0.75$).

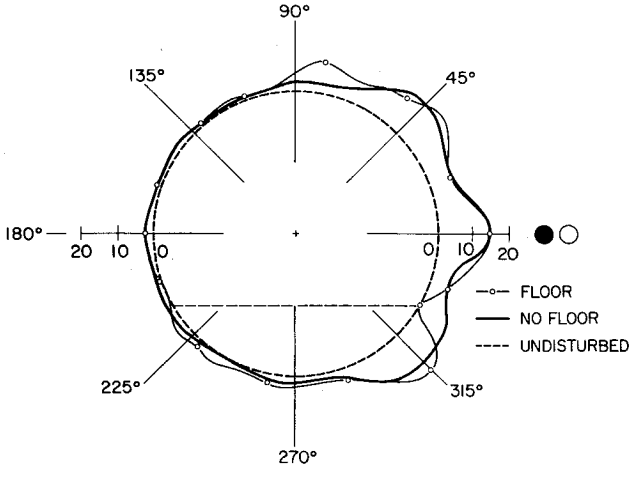

Fig. 6 Shell radial displacement amplitude ($\Omega = 0.4$, $\theta_f = -30$ deg).

modes responding strongly, only the $n = 2$ couples well with the interior acoustic field at this frequency. When the floor is in place, the angular pressure distribution shows little change because, as shown in Table 2, the response of the $n = 2$ structural mode is little affected by the presence of the floor and the higher-order and asymmetric structural modes generated by the floor do not couple well with the interior space.

There has been some suggestion that the internal floor can be used to stiffen the aircraft fuselage selectively in order to reduce noise transmission to the interior. Therefore, it is interesting to simulate this situation by locating the floor at a position of

Table 4 Displacement modal decompositions ($\Omega = 0.4$, $\theta_f = -30$ deg)

	A_n		B_n	
n	No floor	Floor	No floor	Floor
0	0.650×10^{0}	0.650×10^{0}	0	0
1	0.607×10^{0}	0.675×10^{0}	0	0.696×10^{-1}
2	0.179×10^{1}	0.181×10^{1}	0	0.111×10^{0}
3	0.315×10^{1}	0.315×10^{1}	0	0.609×10^{0}
4	0.441×10^{1}	0.421×10^{1}	0	0.767×10^{0}
5	0.408×10^{1}	0.359×10^{1}	0	0.490×10^{0}
6	0.443×10^{1}	0.426×10^{1}	0	0
7	0.314×10^{1}	0.205×10^{1}	0	0.908×10^{0}
8	0.138×10^{1}	0.229×10^{1}	0	0.974×10^{0}
9	0.489×10^{0}	0.489×10^{0}	0	0.105×10^{1}

Table 5 Pressure modal decompositions ($\Omega = 0.4$, $\theta_f = -30$ deg, $r/a = 0.75$)

	A_n		B_n	
n	No floor	Floor	No floor	Floor
0	0.639×10^{-1}	0.108×10^{0}	0	0
1	0.129×10^{-1}	0.982×10^{-1}	0	0.739×10^{-2}
2	0.478×10^{0}	0.330×10^{0}	0	0.295×10^{-1}
3	0.130×10^{0}	0.697×10^{0}	0	0.110×10^{0}
4	0.170×10^{1}	0.185×10^{1}	0	0.175×10^{0}
5	0.364×10^{1}	0.182×10^{1}	0	0.973×10^{-1}
6	0.148×10^{1}	0.460×10^{0}	0	0
7	0.688×10^{0}	0.140×10^{0}	0	0.145×10^{-1}
8	0.231×10^{0}	0.435×10^{-1}	0	0.111×10^{-1}
9	0.669×10^{-1}	0.727×10^{-2}	0	0.722×10^{-2}

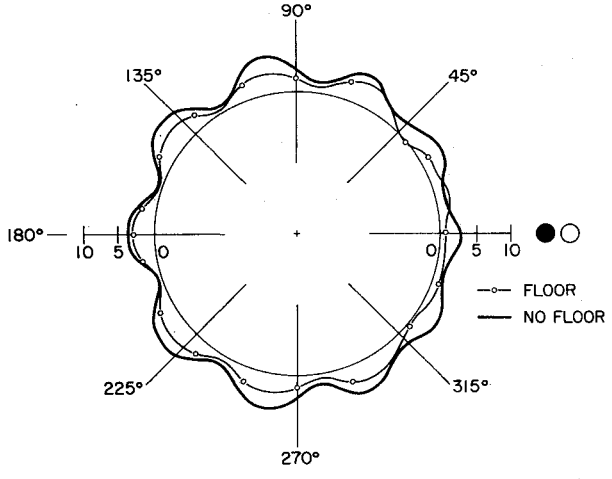

Fig. 7 Shell interior pressure amplitude ($\Omega = 0.4$, $\theta_f = -30$ deg, $r/a = 0.75$).

maximum shell response. Figure 4 shows the displacement distribution of the shell when the floor is located such that $\theta_f = 0$. The driving frequency is $\Omega = 0.2$. In this case, the presence of the floor causes a significant change in the response of the shell and, again, there is zero displacement at the floor location.

On the other hand, Fig. 5 shows the corresponding internal pressure distribution at $r/a = 0.75$ and, again, there is no significant change with the floor in or out. A modal decomposition of the shell and internal pressure response show very similar behavior as demonstrated in the previous tables. Thus, although the floor changes the response of the cylinder, it does so without changing significantly the response of the transmitting mode ($n = 2$). Hence, at this frequency it appears that the floor is of little use in reducing acoustic power flow into the interior. The same may not be true at higher frequencies ($\Omega \gtrsim 0.4$), however.

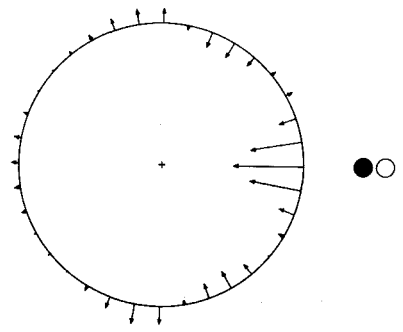

Fig. 8 Radial acoustic intensity with no floor ($\Omega = 0.2$).

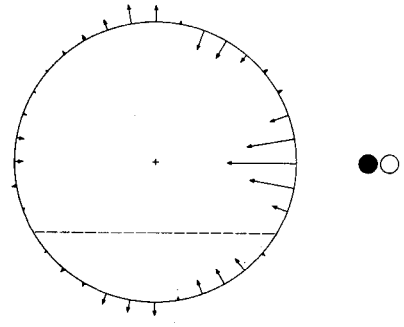

Fig. 9 Radial acoustic intensity ($\Omega = 0.2$, $\theta_f = -30$ deg).

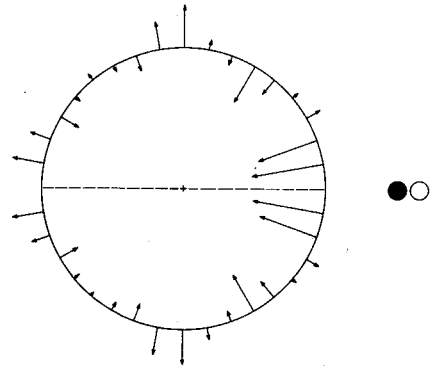

Fig. 10 Radial acoustic intensity ($\Omega = 0.2$, $\theta_f = 0$ deg).

Calculations performed at $\Omega = 0.3$ with a floor angle of $\theta_f = -30$ deg show very similar results to the previous figures. At this frequency, the internal pressure field is dominated by the $n = 3$ mode and is little affected by the presence of the floor.

When the frequency of interest is increased to $\Omega = 0.4$, there is a change in the general behavior of the system. Figure 6 shows the angular distribution of shell displacement and the presence of the floor ($\theta_f = -30$ deg) can be seen to alter the radial response of the cylinder significantly. More importantly, the angular internal pressure distribution, plotted in Fig. 7, is significantly altered at this higher frequency. Overall, the internal levels appear to be reduced in magnitude when the floor is installed. Likewise, Tables 4 and 5 show corresponding displacement and pressure modal decompositions. The modal density of the response of the cylinder with no floor is significantly increased at this higher frequency, and the presence of the floor causes greater scattering of energy into the higher-order and asymmetric shell modes than the lower frequencies. In conjunction, Table 5 indicates that the interior acoustic field is responding strongly in three modes: in other words, the modal density of the interior acoustic field has also significantly increased. When the floor is installed, however, the response of the dominant pressure mode ($n = 5$) is significantly reduced, corresponding to a reduction in the $n = 5$ structural mode. At $\Omega = 0.5$, the floor was also found to alter the internal pressure

levels significantly. However, at this frequency, the internal field is dominated by only one mode, $n = 6$.

Thus, in the frequency range $0 < \Omega \lesssim 0.3$, the floor has little effect on the internal pressure distribution of the cylinder due to the combination of low modal density of the shell and the interior space, and the extensional nature of the shell response in this low-frequency range. For $\Omega \gtrsim 0.4$, the floor appears to have an increasing effect on interior acoustic pressure due to the characteristic change in response of the cylinder from in-plane motion to radial motion near this frequency (see Ref. 10 for a discussion of this behavior), as well as an increased modal density of the interior acoustic space as more acoustic modes are cut on.

Of major concern to reducing interior noise is locating the regions of energy flow into the interior space. Figure 8 gives the distribution of radial intensity at the shell wall interior, calculated using Eq. (9) for $\Omega = 0.2$ and no floor installed. Most of the acoustic energy enters the acoustic space close to $\theta = 0$, or nearest the source. Figure 9 shows the corresponding distribution of radial intensity when a floor is installed at $\theta_f = -30$. Apart from reducing the intensity to zero at the attachment points, the floor has little effect on the distribution of intensity, which is in line with previous results. Integrating the intensity around the circumference allows calculation of the line power (power/unit shell length) at $x/a = 0$. Installing the floor causes no significant reduction in acoustic power flow to the interior for this configuration.

Finally, Fig. 10 shows the intensity vectors when $\theta_f = 0$. In this case, there is some change in the distribution of intensity vectors. In particular, the "hot spot" is reduced to zero at its center. This is to be expected as the intensity is related to both the shell displacement and pressure; however, the line power is reduced by only 1.4 dB when the floor is installed. Interestingly, calculations performed for the case of $\Omega = 0.4$ and 0.5 indicated that the line power is little changed when the floor is installed, even though the pressure amplitude falls significantly at $r/a = 0.75$ in both cases.

Conclusions

The structural effect of the cabin floor on sound transmission into propeller aircraft has been studied using a simplified analytical model. The floor is assumed to force the shell radial displacement to zero at its attachment points. The floor was found to cause scattering of energy into asymmetric and higher-order shell modes. However, for low frequencies ($\Omega \lesssim 0.3$), the floor did not significantly change the internal pressure distribution or amplitude in the source plane. At higher frequencies ($\Omega \gtrsim 0.4$), the floor was found to change significantly the internal pressure distribution. This behavior was shown to be related to the modal density of the shell and contained acoustic field as well as the shell interior space-coupling mechanism, termed interface modal filtering (IMF). The floor was also shown not to change the power flow or intensity distributions significantly into the interior space for all frequencies considered.

Acknowledgments

The author is grateful to NASA Langley Research Center for their support of this research under Grant NAGI-390.

References

[1]Fuller, C. R., "Analytical Model for Investigation of Interior Noise Characteristics in Aircraft with Multiple Propellers including Synchrophasing," *Journal of Sound and Vibration*, Vol. 109, No. 1, 1986, pp. 141–156.

[2]Fuller, C. R., "Mechanisms of Transmission and Control of Low-Frequency Sound in Aircraft Interiors," SAE Paper 850879, 1985.

[3]Fuller, C. R., "Noise Control Characteristics of Synchrophasing—An Analytical Investigation," AIAA Paper 84-2369, 1984.

[4]Jones, J. D. and Fuller, C. R., "Noise Control Characteristics of Synchrophasing—An Experimental Investigation," AIAA Paper 84-2370, 1984.

[5]Johnston, J. L., Donham, R. E., and Guinn, W. A., "Propeller Signatures and Their Use," AIAA Paper 80-1035, 1980.

[6]Pope, L. D., Wilby, E. G., Willis, C. M., and Mayes, W. H., "Aircraft Interior Noise Models: Sidewall Trim, Stiffened Structures, and Cabin Acoustics with Floor Partition," *Journal of Sound and Vibration*, Vol. 89, No. 3, 1983, pp. 371–417.

[7]James, J. H., "Computation of Acoustic Power, Vibration Response and Acoustic Pressure of Fluid-Filled Pipes," Admiralty Marine Technology Establishment, England, Tech. Memo TM82036, 1982.

[8]Jones, J. D. and Fuller, C. R., "Effects of an Internal Floor on Low Frequency Sound Transmission into Aircraft Cabins—An Experimental Investigation," AIAA Paper 86-1939, 1986.

[9]Pope, L. D., "Propeller Aircraft Interior Noise Model-Utilization Study and Validation," NASA CR 172428, 1984.

[10]Fuller, C. R., "The Effects of Wall Discontinuities on the Propagation of Flexural Waves in Cylindrical Shells," *Journal of Sound and Vibration*, Vol. 75, No. 2, 1981, pp. 207–228.

Notice to Subscribers

We apologize that this issue was mailed to you late. As you may know, AIAA recently relocated its headquarters staff from New York, N.Y. to Washington, D.C., and this has caused some unavoidable disruption of staff operations. We will be able to make up some of the lost time each month and should be back to out normal schedule, with larger issues, in just a few months. In the meanwhile, we appreciate your patience.